Available online at www.sciencedirect.com
SCIENCE DIRECT®
Journal of Sound and Vibration 292 (2006) 676–693
JOURNAL OF SOUND AND VIBRATION
www.elsevier.com/locate/jsvi

Dynamic response of a two-level catenary to a moving load

A.V. Metrikine*, A.L. Bosch

Faculty of Civil Engineering and Geosciences, Delft University of Technology, P.O. Box 5048, 2600 GA Delft, The Netherlands

Received 4 June 2004; received in revised form 16 August 2005; accepted 24 August 2005
Available online 7 November 2005

Abstract

An analytical method is proposed for calculating the steady-state response of a two-level catenary to a uniformly moving pantograph. The model for the catenary is composed of two strings (the contact and carrying cables) connected by lumped mass-spring-dashpot elements (hangers), which are positioned equidistantly along the strings. The upper string (carrying cable) is fixed at periodically spaced points. This model is capable of describing a coupled wave dynamics of both the carrying cable and the contact cable of the catenary. The pantograph is modelled by a point load, which moves uniformly along the contact cable. Using the proposed method, the steady-state deflection of the contact cable is analyzed thoroughly. Additionally, the contact force between the hangers and the contact cable is studied, which is important for estimation of the fatigue life of the hangers. Two simplified models of the two-level catenary are introduced and studied. The first model assumes that the carrying cable is infinitely stiff, whereas the second model disregards the discrete character of the hangers. Predictions of these simplified models are compared to those of the original model.

1. Introduction

Overhead catenary systems for high-speed trains require a relatively high tension of both the carrying cable (carrier) and the contact cable. This is needed to prevent the train velocity from getting close to the wave speed of flexural waves in the catenary. It was measured, however, that a higher tension leads to a higher contact loss ratio of the pantograph. To avoid this effect, which leads to a lower efficiency of the current collection, it was proposed to replace conventional droppers (simple cables, on which the contact wire is suspended) by more sophisticated rubber damping hangers or friction damping hangers [1]. These hangers have certain stiffness, viscosity and mass, which can be tuned to minimize wave reflection from the hangers. According to Ref. [1], such tuning allows to reduce the contact loss ratio.

Introduction of the hangers, which are much stiffer in compression than the conventional droppers (the latter have nearly zero stiffness in compression), leads to much more intense an interaction between the cables of the catenary under the pantograph, whose influence is mainly compressive. To account for this interaction, coupled vibrations of the cables should be considered.

*Corresponding author. Faculty of Civil Engineering and Geosciences, Delft University of Technology, Stevinweg 1, 2628 CN Delft, The Netherlands. Tel.: +0152784749; fax: +0152785767.
E-mail address: A.Metrikine@citg.tudelft.nl (A.V. Metrikine).

0022-460X/$ - see front matter © 2005 Elsevier Ltd. All rights reserved.
doi:10.1016/j.jsv.2005.08.026

In this paper, an analytical method is proposed for obtaining the steady-state response of a two-level catenary to a uniformly moving pantograph. The model for the catenary is composed of two strings connected by lumped mass-spring-dashpot elements (hangers). This model is capable of describing a coupled wave dynamics of both the carrying cable and the contact cable. The pantograph is modelled by a point load of a constant or a harmonically varying with time magnitude. Adopting this model of the pantograph, it is implicitly assumed that regardless of the pantograph velocity, the coupled vibrations of the pantograph–catenary system are stable and the steady-state vibrations of this system exist. As shown by Metrikine and Verichev [2], the stable interaction can always be achieved by a proper choice of the effective mass, stiffness and viscosity of the pantograph (the viscosity is the most influential parameter in this case). Note that in this paper the existence of the stable interaction is assumed but the pantograph parameters, which would ensure this, are not determined.

The emphasis of this study is placed on the deflection of the contact cable and its dependence on the load speed. Additionally, the contact force between the hangers and the contact cable is discussed. To reveal significance of the coupling between the two cables, which takes place by means of the lumped hangers, the response of the two-level catenary is compared to that of two simplified models. In the first simplified model the carrying cable is assumed infinitely stiff but effective parameters of the droppers are introduced to account for the stiffness and damping properties of this cable. In the second model, the simplification is concerned with the hangers, which are 'continualized', forming a continuous and homogeneous visco-elastic connection between the two cables.

All three models, which are considered in this paper, belong to a class of periodically inhomogeneous, continuous elastic systems. Such systems, being excited by a uniformly moving load, can respond in a resonance manner at several load velocities. This effect has been studied in the past by a number of researchers employing different but closely related methods. Mead and Jezequel based their approach on the Fourier-series techniques [3–6]. Bogacz, Krzyzinski and Popp applied the Flouquet theorem [7,8]. Vesnitskiy, Metrikine and Belotserkovskiy employed a so-called periodicity condition [9–11]. More references on this subject can be found in the book of Frýba [12].

As compared to the above-mentioned studies, this paper treats an elastic system, which has not one but two spatial periods. The larger period is introduced by the fixations of the carrying cable, whereas the smaller period is associated with the droppers. Additionally, the two-level catenary combines two strongly coupled elastic systems (strings) with different wave speeds. To the authors' knowledge, the steady-state response of such a system to a moving load has not been studied in the past.

The 'periodicity condition method' is applied in this paper, although the other methods could be applied as well. This method is chosen since, in the opinion of the authors, it is elegant, can be interpreted physically, can be generalized to analyze three-dimensional periodically inhomogeneous systems [13,14] and even can be used to find the steady-state response of a layer of regularly positioned discrete particles [15].

This paper is structured in the following manner. In Section 2, a system of equations is presented that governs the transverse motion of the two-level catenary. This system is then transformed into the frequency domain, in which the steady-state solution is obtained in a closed form by employing the periodicity condition. This solution can be transformed into the time domain by using any conventional numerical-inversion technique. In Section 3, results are presented of the numerical analysis of the displacement of the contact cable and of the contact force between a hanger and this cable. In Sections 4 and 5, the simplified models for the catenary are introduced and the steady-state solutions for both these models are obtained in the frequency domain. In Section 6 a comparative study is carried out of the predictions of the original two-level model to those of the simplified models. Section 7 presents main conclusions, which can be drawn from this study.

2. Governing equations and the solution in the frequency domain

The model for a two-level catenary is composed of two parallel, infinitely long strings as depicted in Fig. 1. The upper string (the carrying cable) is fixed at periodically spaced fixation points $x = mD + d/2$, $m = 0, \pm 1, \pm 2, \ldots$, whereas the lower string (the contact wire) is suspended from the upper string by means of lumped mass-spring-dashpot elements (the suspension rods), which are placed periodically at $x = nd$, $n = 0, \pm 1, \pm 2, \ldots$ along the strings. The system in question is subject to a point load (the current collector),

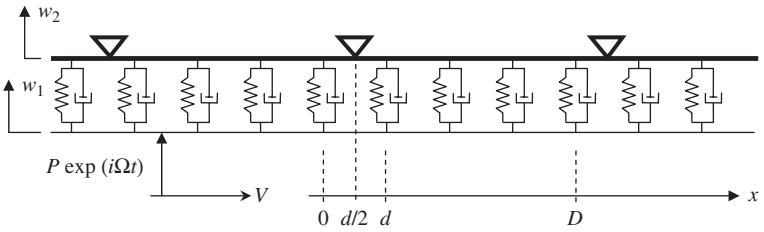

Fig. 1. Two-level catenary under moving load.

which is applied to the lower string. This load moves along the strings with a constant speed and oscillates in time harmonically.

The equations, which govern the small vertical motion of the system about its equilibrium, are given as

$$\rho_1 A_1 \partial_{tt} w_1 - T_1 \partial_{xx} w_1 = P \exp(\mathrm{i}\Omega t)\delta(x - vt), \quad -\infty < x < \infty, \quad x \neq nd, \tag{1}$$

$$\rho_2 A_2 \partial_{tt} w_2 - T_2 \partial_{xx} w_2 = 0, \quad -\infty < x < \infty, \; x \neq nd, \quad x \neq d/2 + mD, \tag{2}$$

$$T_1(\partial_x w_1|_{x=nd+0} - \partial_x w_1|_{x=nd-0}) = ((k_0 + c_0\partial_t)(w_1 - w_2) + m_0\partial_{tt} w_1)_{x=nd}, \tag{3}$$

$$T_2(\partial_x w_2|_{x=nd+0} - \partial_x w_2|_{x=nd-0}) = ((k_0 + c_0\partial_t)(w_2 - w_1) + m_0\partial_{tt} w_2)_{x=nd}, \tag{4}$$

$$(w_1|_{x=nd+0} - w_1|_{x=nd-0}) = (w_2|_{x=nd+0} - w_2|_{x=nd-0}) = 0, \tag{5}$$

$$w_2|_{x=d/2+mD} = 0. \tag{6}$$

Eqs. (1) and (2) govern the motion of the strings everywhere but at the suspension and fixation points. Eqs. (3) and (4) give the dynamic equilibrium of vertical forces at the suspension points. Eq. (5) is the continuity conditions at the suspension points. Eq. (6) describes the fixation of the upper wire.

In Eqs. (1)–(6), subscripts '1' and '2' are related to the lower wire and the upper wire, respectively; $w_j, j = 1, 2$ are the vertical deflections of the strings; ρ_j, A_j and T_j are the material density, the cross-sectional area and the tension of the strings; k_0, c_0 and m_0 are the stiffness, the damping coefficient and the half-mass of the suspension rods; P, V and Ω are the amplitude, the speed and the cyclic frequency of the load; D and d are the spatial periods of the fixation points and the suspension points, respectively; ∂_t and ∂_x imply the partial derivatives with respect to time and the horizontal co-ordinate, respectively; $\delta(\ldots)$ is the Dirac delta function, m and n are integers.

The model for a two-level catenary that is depicted in Fig. 1 is *periodically inhomogeneous*, e.g. its parameters vary periodically with the co-ordinate x. Thus, this model can exhibit the steady-state response under a harmonically oscillating load that moves along the strings with a constant speed. This response can be found with the help of a so-called periodicity condition [9–11], which must be satisfied in the steady-state regime. For the model in question, this condition reads

$$w_j(x, t) = w_j\left(x + mD, \; t + \frac{mD}{V}\right)\exp\left(\frac{-\mathrm{i}\Omega mD}{V}\right). \tag{7}$$

Physically, the periodicity condition implies that the displacement pattern of the strings repeats itself in time with the period D/V simultaneously undergoing the spatial translation D and the phase shift $\Omega d/V$. In mathematical terms, Eq. (7) presents a transformation of variables, with respect to which the governing equations are invariant as long as the initial conditions are not accounted for.

The steady-state solution to Eqs. (1)–(6) can be obtained analytically by transforming the problem into the frequency domain. This transformation is carried out with the help of the following integral Fourier transform:

$$w_j^{(\omega)}(x, \omega) = \int_{-\infty}^{\infty} w_j(x, t)\exp(\mathrm{i}\omega t)\,\mathrm{d}t. \tag{8}$$

Application of this transform to Eqs. (1)–(7) gives

$$\partial_{xx} w_1^{(\omega)} + \frac{\omega^2}{c_1^2} w_1^{(\omega)} = -\frac{P}{T_1 V} \exp\left(\frac{\mathrm{i}(\Omega+\omega)}{V} x\right), \quad -\infty < x < \infty, \ \ x \neq nd, \tag{9}$$

$$\partial_{xx} w_2^{(\omega)} + \frac{\omega^2}{c_2^2} w_2^{(\omega)} = 0, \quad -\infty < x < \infty, \ \ x \neq nd, \ \ x \neq d/2 + mD, \tag{10}$$

$$T_1(\partial_x w_1^{(\omega)}|_{x=nd+0} - \partial_x w_1^{(\omega)}|_{x=nd-0}) = ((k_0 - \mathrm{i}\omega c_0)(w_1^{(\omega)} - w_2^{(\omega)}) - m_0\omega^2 w_1^{(\omega)})_{x=nd}, \tag{11}$$

$$T_2(\partial_x w_2^{(\omega)}|_{x=nd+0} - \partial_x w_2^{(\omega)}|_{x=nd-0}) = ((k_0 - \mathrm{i}\omega c_0)(w_2^{(\omega)} - w_1^{(\omega)}) - m_0\omega^2 w_2^{(\omega)})_{x=nd}, \tag{12}$$

$$(w_1^{(\omega)}|_{x=nd+0} - w_1^{(\omega)}|_{x=nd-0}) = 0, \tag{13}$$

$$(w_2^{(\omega)}|_{x=nd+0} - w_2^{(\omega)}|_{x=nd-0}) = 0, \tag{14}$$

$$w_2^{(\omega)}|_{x=d/2+mD} = 0, \tag{15}$$

$$w_j^{(\omega)}(x,\omega) = w_j^{(\omega)}(x+mD,\omega) \exp\left(\frac{-\mathrm{i}(\Omega+\omega)mD}{V}\right), \tag{16}$$

where $c_j = \sqrt{T_j/(\rho_j A_j)}$ are the wave speeds in the strings.

To obtain the solution to the problem governed by Eqs. (9)–(15), which satisfies the periodicity condition (16), the following steps will be undertaken. Firstly, the general solution to Eqs. (9) and (10) will be written in the interval $x \in [0, D]$. This solution will contain $4N_s + 2$ unknown coefficients, N_s being the number of suspension rods between two neighboring fixation points (every 'free' segment of the string will generate two constants, which correspond to the complex amplitudes of waves propagating leftward and rightward in this segment). Secondly, this solution will be 'extended' to the interval $x \in [D, 2D]$ by employing the periodicity condition (16). The solution in the latter interval will contain the same unknown coefficients. Finally, these coefficients will be found with the help of the boundary conditions at the suspension and fixation points, Eqs. (11)–(15).

The general solution to Eqs. (9) and (10) in the interval $x \in [0, D]$ can be written as

$$(n-1)d \leqslant x \leqslant nd, \quad 1 \leqslant n \leqslant N_s$$

$$w_1^{(\omega)} = C_{2n-1} \exp\left(\frac{\mathrm{i}\omega x}{c_1}\right) + C_{2n} \exp\left(-\frac{\mathrm{i}\omega x}{c_1}\right) + C_{\mathrm{part}} \exp\left(\frac{\mathrm{i}(\omega+\Omega)x}{V}\right), \tag{17}$$

$$0 \leqslant x \leqslant d/2:$$

$$w_2^{(\omega)} = C_{2N_s+1} \exp\left(\frac{\mathrm{i}\omega x}{c_2}\right) + C_{2N_s+2} \exp\left(-\frac{\mathrm{i}\omega x}{c_2}\right), \tag{18}$$

$$d/2 + (n-1)d \leqslant x \leqslant nd, \quad 1 \leqslant n \leqslant N_s:$$

$$w_2^{(\omega)} = C_{2N_s+2n+1} \exp\left(\frac{\mathrm{i}\omega x}{c_2}\right) + C_{2N_s+2n+2} \exp\left(-\frac{\mathrm{i}\omega x}{c_2}\right) \tag{19}$$

with

$$C_{\mathrm{part}} = \frac{PV}{T_1} \frac{1}{(\Omega+\omega)^2 - \omega^2 V^2/c_1^2}. \tag{20}$$

Employing the periodicity condition (16), the general solution, (17)–(19), can be used to write the solution in the interval $x \in [D, 2D]$. For the analysis to follow, it is sufficient to express $w_1^{(\omega)}$ for $D \leqslant x \leqslant D + d$ and $w_2^{(\omega)}$

for $D \leqslant x \leqslant D + d/2$. These expressions read

$$w_1^{(\omega)} = \exp\left(\frac{\mathrm{i}(\Omega+\omega)D}{V}\right)\left(C_1 \exp\left(\frac{\mathrm{i}\omega(x-D)}{c_1}\right) + C_2 \exp\left(-\frac{\mathrm{i}\omega(x-D)}{c_1}\right)\right) + C_{\mathrm{part}} \exp\left(\frac{\mathrm{i}(\Omega+\omega)x}{V}\right), \tag{21}$$

$$w_2^{(\omega)} = \exp\left(\frac{\mathrm{i}(\Omega+\omega)D}{V}\right)\left(C_{2N_s+1} \exp\left(\frac{\mathrm{i}\omega(x-D)}{c_2}\right) + C_{2N_s+2} \exp\left(-\frac{\mathrm{i}\omega(x-D)}{c_2}\right)\right), \tag{22}$$

Substituting Eqs. (17)–(19) and Eq. (21) into the boundary conditions (11)–(15), a system of $4N_s + 2$ linear algebraic equations can be obtained with respect to unknown coefficients C_k, $1 \leqslant k \leqslant 4N_s + 2$. More specifically, the following substitutions have to be made:

- Eqs. (17) and (19) are to be substituted into Eqs. (11)–(14) with $1 \leqslant n \leqslant N_s - 1$ to give the following $4N_s - 4$ equations:

$$-\alpha_1^n(a+\beta_1)C_{2n-1} + \alpha_1^{-n}(\beta_1 - a)C_{2n} + \alpha_1^n\beta_1 C_{2n+1} - \alpha_1^{-n}\beta_1 C_{2n+2} + b\alpha_2^n C_{2N_s+2n+1} + b\alpha_2^{-n} C_{2N_s+2n+2} = aC_{\mathrm{part}}\alpha_f^n, \quad 1 \leqslant n \leqslant N_s - 1, \tag{23}$$

$$-\alpha_2^n(a+\beta_2)C_{2N_s+2n+1} + \alpha_2^{-n}(\beta_2 - a)C_{2N_s+2n+2} + \alpha_2^n\beta_2 C_{2N_s+2n+3} - \alpha_2^{-n}\beta_2 C_{2N_s+2n+4} + b\alpha_1^n C_{2n-1} + b\alpha_1^{-n} C_{2n} = -bC_{\mathrm{part}}\alpha_f^n, \quad 1 \leqslant n \leqslant N_s - 1, \tag{24}$$

$$-\alpha_1^n C_{2n-1} - \alpha_1^{-n} C_{2n} + \alpha_1^n C_{2n+1} + \alpha_1^{-n} C_{2n+2} = 0, \quad 1 \leqslant n \leqslant N_s - 1, \tag{25}$$

$$-\alpha_2^n C_{2N_s+2n+1} - \alpha_2^{-n} C_{2N_s+2n+2} + \alpha_2^n C_{2N_s+2n+3} + \alpha_2^{-n} C_{2N_s+2n+4} = 0, \quad 1 \leqslant n \leqslant N_s - 1, \tag{26}$$

- Eqs. (17) and (19) with $x = dN_s = D$ and Eqs. (21)–(22) are to be substituted into Eqs. (11)–(14) to give the following four equations:

$$-\alpha_1^{N_s}(a+\beta_1)C_{2N_s-1} + \alpha_1^{-N_s}(\beta_1 - a)C_{2N_s} + \alpha_f^{N_s}\beta_1 C_1 - \alpha_f^{N_s}\beta_1 C_2 + b\alpha_2^{N_s} C_{4N_s+1} + b\alpha_2^{-N_s} C_{4N_s+2} = aC_{\mathrm{part}}\alpha_f^{N_s}, \tag{27}$$

$$-\alpha_2^{N_s}(a+\beta_2)C_{4N_s+1} + \alpha_2^{-N_s}(\beta_2 - a)C_{4N_s+2} + \alpha_f^{N_s}\beta_2 C_{2N_s+1} - \alpha_f^{N_s}\beta_2 C_{2N_s+2} + b\alpha_1^{N_s} C_{2N_s-1} + b\alpha_1^{-N_s} C_{2N_s} = -bC_{\mathrm{part}}\alpha_f^{N_s}, \tag{28}$$

$$-\alpha_1^{N_s} C_{2N_s-1} - \alpha_1^{-N_s} C_{2N_s} + \alpha_f^{N_s} C_1 + \alpha_f^{N_s} C_2 = 0, \tag{29}$$

$$-\alpha_2^{N_s} C_{4N_s+1} - \alpha_2^{-N_s} C_{4N_s+2} + \alpha_f^{N_s} C_{2N_s+1} + \alpha_f^{N_s} C_{2N_s+2} = 0. \tag{30}$$

- $w_2^{(\omega)}$ should be set to zero at $x = d/2$ to give the last two equations:

$$\alpha_2^{1/2} C_{2N_s+1} + \alpha_2^{-1/2} C_{2N_s+2} = 0, \tag{31}$$

$$\alpha_2^{1/2} C_{2N_s+3} + \alpha_2^{-1/2} C_{2N_s+4} = 0. \tag{32}$$

In Eqs. (23)–(32), the following notations are used:

$$\alpha_j = \exp\left(\frac{\mathrm{i}\omega d}{c_j}\right), \quad \alpha_f = \exp\left(\frac{\mathrm{i}(\Omega+\omega)d}{V}\right), \quad \beta_j = \frac{\mathrm{i}\omega T_j}{c_j}, \quad j = 1, 2,$$
$$a = k_0 - \mathrm{i}\omega c_0 - m_0\omega^2, \quad b = k_0 - \mathrm{i}\omega c_0.$$

The system of linear algebraic equations with respect to the coefficients C_k, $1 \leqslant k \leqslant 4N_s + 2$, Eqs. (23)–(32), can be readily solved numerically given parameters of the system and the frequency ω. Substituting these coefficients into Eqs. (17)–(19), the steady-state response of the cables in the frequency domain can be determined in the interval $x \in [0, D]$. The response outside this interval can be easily found with the help of the periodicity condition (16). To determine the response of the cables in the time domain, the inverse Fourier transform over the frequency ω should be applied. Some results of this inversion are presented and discussed in the next section taking example of a catenary with $N_s = 7$.

3. The steady-state response of the catenary

In this section, the steady-state dynamic response of the contact cable is studied. Additionally, the contact force is discussed between the contact cable and the suspension rods.

The response of the catenary is calculated using parameters shown in Table 1. The parameters of the suspension rods correspond to so-called *friction damping hangers* and *rubber damping hangers*, which are being currently tested with the aim to replace conventional suspension cables of the overhead power lines for high-speed trains. The main difference between these hangers is their stiffness. The friction hanger is more than 10 times softer than the rubber hanger.

Fig. 2 shows the deflection pattern of the contact cable at the time moment when the load is at the position $x = 3.5\,d$, precisely in the middle of the first span $0 \leqslant x \leqslant D$, which is located between the fixation points $x = 0$ and D. The positions of these and other relevant fixation points are indicated by vertical solid lines at the top of the figures. Each figure presents the deflection of the contact cable for a given velocity of the load. The deflection is plotted both for the friction and rubber hangers.

Figs. 2(a)–(d) show the deflection of the cable caused by the constant load ($\Omega = 0$). Fig. 2(a) corresponds to the load velocity, which is about a half of the wave speeds in the cables. In this case, the cable deflection pattern is quasi-symmetric in the vicinity of the load, but is obviously asymmetric at a larger scale. This asymmetry is caused by radiation of elastic waves by a constant load as it moves along a periodically inhomogeneous system [10]. As shown in [10], transverse elastic waves are excited in the cables every time that the load passes a suspension point. The excited waves form two pulses, one propagating rightward and the other leftward along the catenary. Both pulses have continuous spectra, containing all frequencies. Since the load moves uniformly, it excites these pulses regularly while passing through each suspension point. This

Table 1
Parameters of the model

Geometry			
Distance between fixation points	Number of suspension points	Distance between suspension points	
$D = 50\,\mathrm{m}$	$N_s = 7$	$d = D/N_s = 7.1428\,\mathrm{m}$	
Cables		Suspension rods	
Contact cable	Carrying cable	Friction damping hanger	Rubber damping hanger
$T_1 = 19600\,\mathrm{N}$ $\rho_1 A_1 = 2.175\,\mathrm{kg/m}$ $\sigma_1 = T_1/A_1 = 145\,\mathrm{N/mm^2}$ $c_1 = 94.93\,\mathrm{m/s}$	$T_1 = 9800\,\mathrm{N}$ $\rho_1 A_1 = 1.5\,\mathrm{kg/m}$ $\sigma_2 = T_2/A_2 = 58\,\mathrm{N/mm^2}$ $c_2 = 80.83\,\mathrm{m/s}$	$k_0 = 1500\,\mathrm{N/m}$ $c_0 = 50\,\mathrm{Ns/m}$ $m_0 = 0.2\,\mathrm{kg}$	$K_0 = 55000\,\mathrm{N/m}$ $c_0 = 85\,\mathrm{Ns/m}$ $m_0 = 0.2\,\mathrm{kg}$

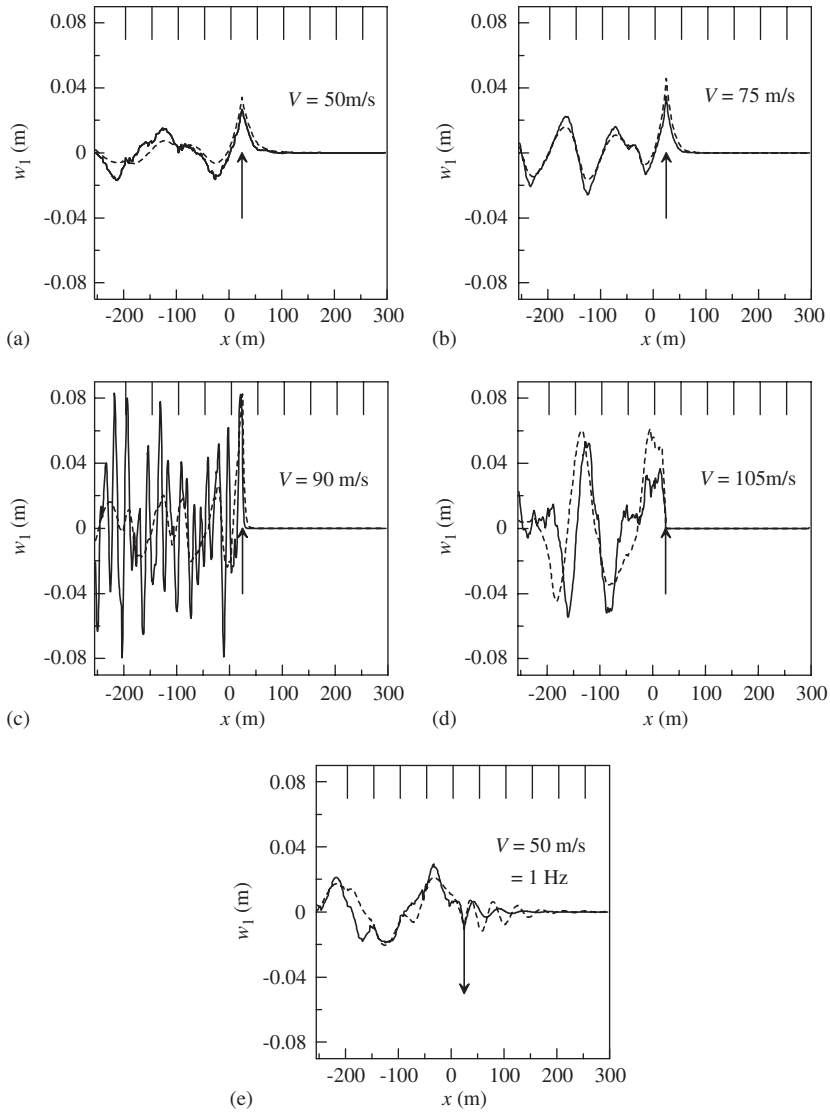

Fig. 2. Displacement patterns of the two-level catenary. (a) $V = 50\,\mathrm{m/s}$, (b) $V = 75\,\mathrm{m/s}$, (c) $V = 90\,\mathrm{m/s}$, (d) $V = 105\,\mathrm{m/s}$, (e) $V = 50\,\mathrm{m/s}$ and $\Omega = 1\,\mathrm{Hz}$. Solid line: rubber hangers; dashed line: friction hangers.

regularity implies that some harmonic components of these pulses amplify each other being radiated precisely in phase. In the steady-state regime (after a sufficiently long time), the contribution of these harmonics into the vibration of the catenary becomes prevailing so that the spectrum of this vibration becomes almost discrete (or completely discrete if no damping is accounted for). The peaks of this spectrum correspond to the harmonics, which are excited in phase at each suspension point and are distinguished by the condition that their phase velocity equals the velocity of the load (in the case that $\Omega = 0$). It should be noted that there are infinitely many harmonic components that satisfy this condition since in the periodically inhomogeneous systems infinitely many waves with different wavelengths may propagate having the same frequency. Conventionally, the wave with the shortest wavelength is referred to as the main harmonic, whereas all other waves are called the super-harmonics. A comprehensive discussion of elastic wave radiation in inhomogeneous systems under moving loads can be found in the review of Vesnitskiy and Metrikine [10].

The effect of the hangers' type in Figs. 2(a)–(d) is not pronounced, although the friction hangers lead to a smother shape of the cable. This is natural, since the friction hangers are much softer and cannot give rise to sharp variations of the deflection pattern.

Fig. 2(b) shows the cable deflection for somewhat higher load velocity: $V/c_1 \approx 0.79$, $V/c_2 \approx 0.93$. Comparing Figs. 2(a) and 2(b), it can be seen that as the load velocity gets closer to the wave speeds, the deflection of the cable grows and the waves behind the load become shorter, in correspondence with the Doppler Effect. The effect of the hangers is not significant like in the previous case.

Fig. 2(c) presents the deflection pattern for $V/c_1 \approx 0.95$, $V/c_2 \approx 1.11$. This implies that the load moves just a little slower than the waves in the contact cable and somewhat faster than the waves in the carrying cable. The response of the contact cable grows significantly in this case, which is in correspondence with a general rule that the closer the load velocity to a wave speed, the higher is the response. The waves behind the load shorten tremendously, complying with the Doppler Effect, which dictates that if $V \to c$, then the wavelength of radiated waves must tend to zero. The deflection pattern becomes asymmetric not only at a large scale but also in the vicinity of the load. This is one of the consequences of a quasi-super-critical motion of the load ('quasi' implies here that the load velocity exceeds the wave speed only in the carrying cable). The contact cable in front of the load is disturbed only in the very vicinity of the load. This disturbance is solely due to propagation of waves in the contact cable. The effect of the hangers is perceptible: the friction (soft) hangers lead to almost twice smaller the wave amplitude behind the load. This result is completely against a 'static' expectation that the response of a softer system should be larger. Such an expectation, however, is not applicable if the load moves with almost the wave speed.

Fig. 2(d) corresponds to a super-critical load motion with $V/c_1 \approx 1.11$, $V/c_2 \approx 1.3$. In this case, the contact cable in front of the load is not disturbed at all in correspondence with the Mach and Cherenkov Effects [16]. The maximum deflection is lower than in the previous case because of a larger difference between the load velocity and the wave speed. The wave pattern behind the load in this case is composed both of the primary wave, which would exist in a corresponding homogeneous system, and a number of super-harmonics caused by the periodic inhomogeneity. The effect of the hangers' type on the deflection amplitude is not pronounced, but the stiffer rubber hangers cause a very irregular deflection of the contact cable.

Fig. 2(e) presents the cable response to a harmonically varying load that moves relatively slowly with the velocity $V = 50\,\mathrm{m/s}$. Comparing this figure to Fig. 2(a), it can be seen that the harmonic load causes somewhat more pronounced and wavy response in front of the load. The cable pattern behind the load remains qualitatively the same.

To take a closer look at the loading point, around which the highest deflections may be expected in the sub-critical regime of motion, the load path (the deflection of the contact cable at the loading point) is shown in Fig. 3 as a function of the load position within the first span $0 \leqslant x \leqslant D$. In correspondence with the periodicity condition (7), this path, for the load of a constant magnitude, is repetitive with the period D. Three velocities of the load ($\Omega = 0$) are considered: $V = 50,\ 75,\ 90\,\mathrm{m/s}$, which correspond to the cable deflections shown in Figs. 2(a–c). The load path for $V = 105\,\mathrm{m/s}$ is not shown since in this case the deflection under the load is trivially zero.

Fig. 3 shows that the load path is asymmetric with respect to the middle point of the span, $x = 25\,\mathrm{m}$. This asymmetry is associated with wave radiation (caused by the system inhomogeneity), which takes place at *any*

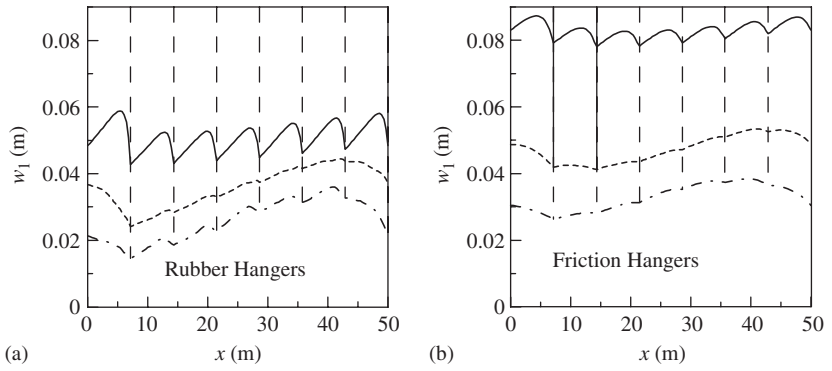

Fig. 3. Deflection of the contact cable of the two-level catenary at the loading point. (a) Rubber hangers, (b) friction hangers. Dashed—dotted line: $V = 50\,\mathrm{m/s}$; dashed line: $V = 75\,\mathrm{m/s}$; solid line: $V = 90\,\mathrm{m/s}$.

load velocity not equal to zero [10]. Thus, the load path must be asymmetric for all load velocities. The degree of this asymmetry, however, depends on the load velocity. The closer the load velocity to the wave speed, the more asymmetric is the load path.

According to Fig. 3, the load path changes sharply as the load passes a hanger (positions of the hangers are indicated by the vertical dashed lines). For the rubber hangers this change is more pronounced than for the friction hangers, since the former hangers are stiffer. The path between two hangers is asymmetric with respect to the middle point and the maximum deflection is reached somewhat closer to the hanger, toward which the load moves. The faster the load moves, the closer this maximum is to this hanger. The load path corresponding to $V = 90\,\mathrm{m/s}$ is almost repetitive at every inter-hanger interval. This is because the load velocity is almost equal to the wave speed in the contact cable. In this case, the interaction of the load and the catenary takes place quasi-locally, around the loading point. Consequently, there are perceptible pieces of the contact cable, which follow every hanger, where the deflection increases almost linearly, as if the contact cable were not suspended on the hangers.

The last interesting observation to be made from Fig. 3 is related to the magnitude of the deflection under the load in the case $V = 90\,\mathrm{m/s}$. Fig. 3 shows that this deflection is perceptibly smaller for the rubber hangers than for the friction hangers. This seems to be in contradiction with Fig. 2(c), which shows that in the vicinity of the load the cable displacement hardly depends on the type of the hangers. This, however, is not a contradiction, but just a consequence of two effects: a very rapid variation of the cable deflection around the load and a fact that the maximum deflection of the cable takes place somewhat behind the loading point. In the case of the rubber hangers, the load is just farther away from the point of maximum deflection than in the case of the friction hangers.

The maximum deflection of the contact cable takes place at a certain distance from the load. Therefore, this deflection should be found by calculating the cable deflection at every point of the span $0 \leqslant x \leqslant D$, varying the time from a large negative value to a sufficiently large positive value. Such a calculation, however, would be very time consuming. In this paper, the maximum deflection of the middle point of the span, $x = 25\,\mathrm{m}$, is studied by varying the time. This is a reasonable approximation of the 'truly maximum deflection' since this point has the lowest stiffness in the static sense.

Fig. 4 presents the maximum deflection of the contact cable under the constant ($\Omega = 0$) load at the point $x = 25\,\mathrm{m}$ as a function of the load velocity both for the friction and rubber hangers. This figure shows that the main dynamic amplification of the cable response takes place at the velocity of the load approximately equal to the wave speed in the contact cable ($c_1 = 94.93\,\mathrm{m/s}$). This is a conventional phenomenon: the closer the load velocity to the wave speed, the higher is the response. In addition to the main amplification at $V = c_1 = 94.93\,\mathrm{m/s}$, Fig. 4 shows a number of resonance peaks corresponding to smaller velocities. Especially pronounced is the peak at $V \approx 30\,\mathrm{m/s}$, which is exhibited by the catenary with rubber hangers. This and the other resonance peaks are associated with super-harmonics, which the load excites in the periodically inhomogeneous catenary. The number of these super-harmonics is infinite (theoretically) and if the group velocity of one of these harmonics approaches the load velocity, a resonance amplification of the response should be expected [5,10]. Due to the damping in the hangers, however, only a few first harmonics, which correspond to lower frequencies, can cause the amplification. The resonance peak at $V \approx 30\,\mathrm{m/s}$ corresponds to the first super-harmonic and is visible for the catenary with both the rubber and friction hangers. The catenary with the rubber hangers exhibits a larger amplification because the damping–stiffness ratio for these hangers is much lower than that for the friction hangers. This is also the reason why the catenary with the rubber hangers shows a number of smaller peaks, which correspond to higher-frequency super-harmonics. In the case of the friction hangers, resonance on these harmonics is damped out.

Thus, the main conclusion to be drawn from Fig. 4 is that the maximum response of a catenary should be expected when the load velocity approaches the wave speed in the contact cable. A number of other critical velocities may be expected, which lead to a perceptible dynamic amplification, especially in the case that the damping–stiffness ratio of the hangers is low.

Designing a catenary, it is important to predict the contact force, which a moving pantograph can generate in the suspension points of the contact cable. In accordance with Eq. (3), this force at the nth hanger is given as

$$F_{\mathrm{susp}} = ((k_0 + c_0\partial_t)(w_1 - w_2) + m_0\partial_{tt}w_1)_{x=nd}. \tag{33}$$

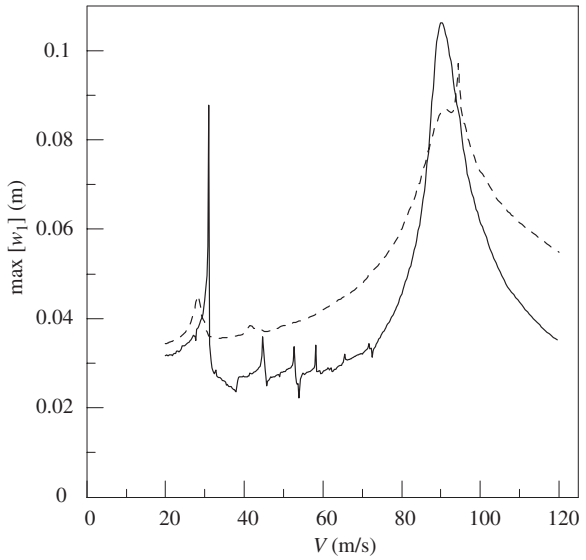

Fig. 4. Maximum deflection of the contact cable of the two-level catenary versus load velocity. Solid line: rubber hangers; dashed line: friction hangers.

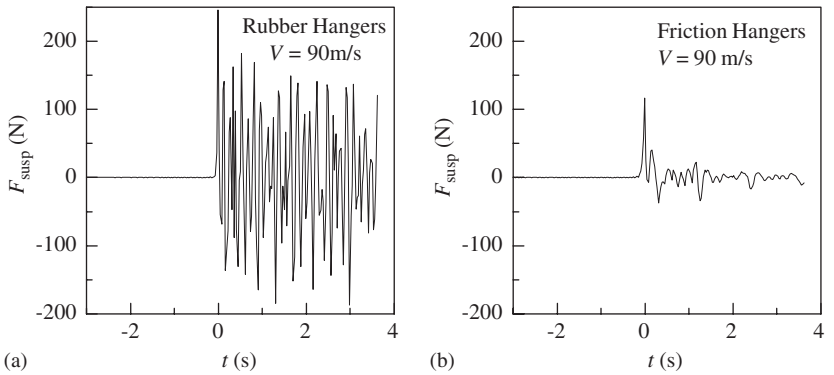

Fig. 5. Time dependence of the contact force between the hanger at $x = 0$ and the contact cable of the two-level catenary. (a) Rubber hangers, (b) friction hangers; $V = 90\,\mathrm{m/s}$.

Fig. 5 shows the contact force at $x = 0$ as a function of time. This position is chosen since the aggregate stiffness of a hanger and the carrying cable increases, as the hanger gets closer to a fixation point of the carrying cable. Accordingly, the contact force can be expected to be higher at this hanger. The contact force is shown in Fig. 5 for the load velocity of 90 m/s, which is very close to the wave speed in the contact cable. In this case, the highest contact force can be expected (as compared to lower or higher velocities of the load). Fig. 5 shows that in this extreme regime the contact force can be four times as high as the load itself if the stiff rubber hangers are used. Important enough is that the contact force keeps oscillating long after the load has passed the suspension point. These oscillations can reduce the fatigue life of the hangers significantly. The softer rubber hangers correspond to almost as twice as moderate contact force and to much less pronounced post-oscillations. This suggests that the fatigue life of the softer hangers should be expected to be perceptibly longer.

Thus, in this section, the steady-state dynamic response of a two-level catenary has been analyzed. To do so, a significant calculation time has been necessary. To reduce this time it makes sense to develop some simplified models of the two-level catenary, which would be capable of relatively quick and accurate prediction of its dynamic response. Two such models are presented and studied in the next sections.

4. Effective one-level model

In this section, an effective one-level model of the catenary is presented, in which the carrying cable is considered as infinitely stiff. To account for the stiffness and the damping associated with the carrying cable, effective parameters of the hangers are introduced.

The model is depicted in Fig. 6. It is composed of an infinitely long string (contact cable), which is suspended by means of lumped mass-spring-dashpot elements, which are placed periodically at $x = nd$, $n = 0, \pm1, \pm2, \ldots$ along the string. The upper ends of these elements are assumed immovable.

The effective stiffness of the mass-spring-dashpot elements is considered to be the stiffness of a sequence of two springs, one having the actual stiffness k_0 of a hanger and the other having the stiffness $4T_2/D$ associated with the carrying cable. The latter stiffness is calculated as the static stiffness of the middle point of a span of the carrying cable, disregarding the suspension rods. The effective damping coefficient of the elements is constructed in a similar manner, as the damping coefficient of a sequence of two dashpots. The first dashpot has the actual damping coefficient c_0 of a hanger, while the second one has the damping coefficient $2T_2/c_2$. The latter coefficient corresponds to the dashpot, by which the reaction of an infinite string (with parameters of the carrying cable) to a point load can be modelled. The effective mass of the effective elements is taken equal to the mass $2m$ of a hanger. Thus, the parameters of the 'effective' hangers are given as

$$k_{\text{eff}} = \frac{4T_2k_0/D}{k_0 + 4T_2/D}, \quad c_{\text{eff}} = \frac{2T_2c_0/c_2}{c_0 + 2T_2/c_2}, \quad m_{\text{eff}} = 2m_{0.} \tag{34}$$

The governing equations for the model at hand read

$$\rho_1 A_1 \partial_{tt} w_1 - T_1 \partial_{xx} w_1 = P \exp(\mathrm{i}\Omega t)\delta(x - vt), \quad -\infty < x < \infty, \ \ x \neq nd, \tag{35}$$

$$T_1(\partial_x w_1|_{x=nd+0} - \partial_x w_1|_{x=nd-0}) = ((k_{\text{eff}} + c_{\text{eff}}\partial_t + m_{\text{eff}}\partial_{tt})w_1)_{x=nd}, \tag{36}$$

$$(w_1|_{x=nd+0} - w_1|_{x=nd-0}) = 0. \tag{37}$$

In this system of equations and in what follows, the same notations are used as in the previous sections.

The steady-state solution of the system of Eqs. (35)–(37) can be found in the same manner as that of the equations which govern the motion of the two-level catenary. The solution procedure is shortly outlined below.

Applying to Eqs. (35)–(37) the Fourier transform defined by Eq. (8), the following system of equations is obtained in the frequency domain:

$$\partial_{xx} w_1^{(\omega)} + \frac{\omega^2}{c_1^2} w_1^{(\omega)} = -\frac{P}{T_1 V} \exp\left(\frac{\mathrm{i}(\Omega + \omega)}{V} x\right), \quad -\infty < x < \infty, \ \ x \neq nd, \tag{38}$$

$$T_1(\partial_x w_1^{(\omega)}|_{x=nd+0} - \partial_x w_1^{(\omega)}|_{x=nd-0}) = ((k_{\text{eff}} - \mathrm{i}\omega c_{\text{eff}} - m_{\text{eff}}\omega^2)w_1^{(\omega)})_{x=nd}, \tag{39}$$

$$(w_1^{(\omega)}|_{x=nd+0} - w_1^{(\omega)}|_{x=nd-0}) = 0. \tag{40}$$

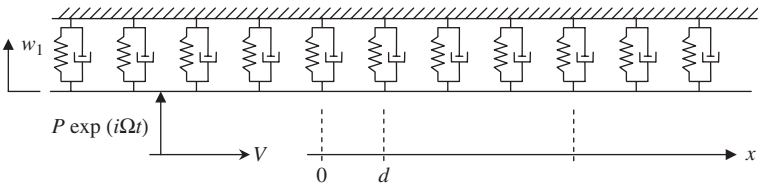

Fig. 6. Effective one-level model of the catenary.

The general solution of Eq. (38) in the interval $x \in [0, d]$ can be written as

$$w_1^{(\omega)} = C_1 \exp\left(\frac{\mathrm{i}\omega x}{c_1}\right) + C_2 \exp\left(-\frac{\mathrm{i}\omega x}{c_1}\right) + C_{\mathrm{part}} \exp\left(\frac{\mathrm{i}(\omega+\Omega)x}{V}\right), \tag{41}$$

where C_{part} is given by Eq. (20).

Employing the periodicity condition, which, for the problem at hand, has the following form:

$$\begin{aligned} w_1(x,t) &= w_1\left(x+nd, t+\frac{nd}{V}\right) \exp\left(\frac{-\mathrm{i}\Omega nd}{V}\right) \\ &\Rightarrow w_1^{(\omega)}(x,\omega) = w_1^{(\omega)}(x+nd,\omega) \exp\left(\frac{-\mathrm{i}(\Omega+\omega)nd}{V}\right), \end{aligned} \tag{42}$$

the solution to Eq. (38) in the interval $x \in [d, 2d]$ can be expressed as

$$w_1^{(\omega)} = \exp\left(\frac{\mathrm{i}(\Omega+\omega)d}{V}\right)\left(C_1 \exp\left(\frac{\mathrm{i}\omega(x-d)}{c_1}\right) + C_2 \exp\left(-\frac{\mathrm{i}\omega(x-d)}{c_1}\right)\right) + C_{\mathrm{part}} \exp\left(\frac{\mathrm{i}(\Omega+\omega)x}{V}\right). \tag{43}$$

Substitution of Eqs. (41) and (42) into the boundary conditions (39), (40) taken at $x = d$, gives a system of two linear algebraic equations with respect to C_1 and C_2. This system can be readily solved analytically. Substituting obtained expressions for C_1 and C_2 into Eq. (41), the steady-state response of the contact cable in the frequency domain can be derived in the interval $x \in [0, d]$. The response outside this interval can be found by using the periodicity condition (42). To return to the time domain the Fourier-inversion should be performed. This will be done in Section 6, where a comparison will be carried out of the dynamic responses of the originally considered two-level catenary, the effective one-level catenary and a homogenized two-level catenary, which is introduced and elaborated in the next section.

5. Homogenized two-level model

In this section, a simplified two-level model of the catenary is presented. Relative to the originally formulated two-level model, the simplification is concerned with the hangers, which are considered here to be uniformly and continuously distributed along the strings.

The governing equations for this model read

$$(\rho_1 A_1 + m_d)\partial_{tt} w_1 - T_1 \partial_{xx} w_1 + (k_d + c_d \partial_t)(w_1 - w_2) = P \exp(\mathrm{i}\Omega t)\delta(x - vt), \quad -\infty < x < \infty, \tag{44}$$

$$(\rho_2 A_2 + m_d)\partial_{tt} w_2 - T_2 \partial_{xx} w_2 + (k_d + c_d \partial_t)(w_2 - w_1) = 0, \quad -\infty < x < \infty, \ \ x \neq d/2 + mD, \tag{45}$$

$$w_2|_{x=d/2+mD} = 0. \tag{46}$$

The parameters of the continuously distributed hangers in Eqs. (44)–(46) are related to the parameters of the lumped hangers by the following self-explanatory relationships:

$$k_d = k_0/d, \quad c_d = c_0/d, \quad m_d = m_0/d. \tag{47}$$

Transformation of Eqs. (44)–(46) into the frequency domain results in the following system of coupled ordinary differential equations with the zero-displacement condition at $x = d/2 + mD$:

$$\partial_{xx}\tilde{w}_1^{(\omega)} + \left(\frac{\omega^2}{c_1^2} - \frac{a_d}{T_1}\right)\tilde{w}_1^{(\omega)} + \frac{b_d}{T_1}\tilde{w}_2^{(\omega)} = -\frac{P}{T_1 V}\exp\left(\frac{\mathrm{i}(\Omega+\omega)}{V}x\right), \quad -\infty < x < \infty, \tag{48}$$

$$\partial_{xx}\tilde{w}_2^{(\omega)} + \left(\frac{\omega^2}{c_2^2} - \frac{a_d}{T_2}\right)\tilde{w}_2^{(\omega)} + \frac{b_d}{T_2}\tilde{w}_1^{(\omega)} = 0, \quad -\infty < x < \infty, \ \ x \neq d/2 + mD, \tag{49}$$

$$w_2^{(\omega)}|_{x=d/2+mD} = 0, \tag{50}$$

where $a_d = k_d - \mathrm{i}\omega c_d - m_d\omega^2$, $b_d = k_d - \mathrm{i}\omega c_d$.

The general solution of this system in the interval $x \in [d/2,\ d/2+D]$ can be written as

$$w_1^{(\omega)} = \sum_{j=1}^{4} C_j \exp(\mathrm{i}\gamma_j x) + C_{\mathrm{part}}^{(1)} \exp\left(\frac{\mathrm{i}(\Omega+\omega)x}{V}\right),$$
$$w_2^{(\omega)} = \sum_{j=1}^{4} q_j C_j \exp(\mathrm{i}\gamma_j x) + C_{\mathrm{part}}^{(2)} \exp\left(\frac{\mathrm{i}(\Omega+\omega)x}{V}\right), \tag{51}$$

where γ_j, q_j and $C_{\mathrm{part}}^{(1,2)}$ can be found as described below.

The wave numbers γ_j are the roots of the following polynomial of order four:

$$\left(\frac{\omega^2}{c_1^2} - \frac{a_d}{T_1} - \gamma_j^2\right)\left(\frac{\omega^2}{c_2^2} - \frac{a_d}{T_2} - \gamma_j^2\right) - \frac{b_d^2}{T_1 T_2} = 0. \tag{52}$$

The coefficients q_j are defined as

$$q_j = \frac{b_d}{T_2} \Big/ \left(\frac{\omega^2}{c_2^2} - \frac{a_d}{T_2} - \gamma_j^2\right) \tag{53}$$

and the coefficients of the particular solutions $C_{\mathrm{part}}^{(1,2)}$ are defined by the following system of linear algebraic equations:

$$-\frac{(\Omega+\omega)^2}{V^2} C_{\mathrm{part}}^{(1)} + \left(\frac{\omega^2}{c_1^2} - \frac{a_d}{T_1}\right) C_{\mathrm{part}}^{(1)} + \frac{b_d}{T_1} C_{\mathrm{part}}^{(2)} = -\frac{P}{T_1 V},$$
$$-\frac{(\Omega+\omega)^2}{V^2} C_{\mathrm{part}}^{(2)} + \left(\frac{\omega^2}{c_2^2} - \frac{a_d}{T_2}\right) C_{\mathrm{part}}^{(2)} + \frac{b_d}{T_2} C_{\mathrm{part}}^{(1)} = 0. \tag{54}$$

Since the system at hand is periodic with the spatial period D, the periodicity condition in the frequency domain reads

$$w_j^{(\omega)}(x,\omega) = w_j^{(\omega)}(x+mD,\omega) \exp\left(\frac{-\mathrm{i}(\Omega+\omega)mD}{V}\right). \tag{55}$$

Employing this condition, the solution of Eqs. (48)–(50) in the interval $x \in [d/2+D,\ d/2+2D]$ can be expressed as

$$w_1^{(\omega)} = \exp\left(\frac{\mathrm{i}(\Omega+\omega)x}{V}\right) \sum_{j=1}^{4} C_j \exp(\mathrm{i}\gamma_j(x-d)) + C_{\mathrm{part}}^{(1)} \exp\left(\frac{\mathrm{i}(\Omega+\omega)x}{V}\right),$$
$$w_2^{(\omega)} = \exp\left(\frac{\mathrm{i}(\Omega+\omega)x}{V}\right) \sum_{j=1}^{4} q_j C_j \exp(\mathrm{i}\gamma_j(x-d)) + C_{\mathrm{part}}^{(2)} \exp\left(\frac{\mathrm{i}(\Omega+\omega)x}{V}\right). \tag{56}$$

To find the unknown coefficients C_j, a system of four algebraic equations has to be formulated. The first two equations of this system can be obtained by substituting $w_1^{(\omega)}$ from Eqs. (51),(56) into the fixation condition, Eq. (50), at $x = d/2$ and $x = d/2 + D$. The other two equations can be obtained by requiring that both the displacement and the slope of the contact cable ($w_1^{(\omega)}$ and $\partial_x w_1^{(\omega)}$) are continuous at $x = d/2 + D$. Solving so-obtained system of equations and substituting resulting C_j into Eqs. (51), the steady-state solution in the frequency domain can be obtained and subsequently transformed into the time domain.

6. Comparison with simplified models

In this section, capabilities of the above-introduced simplified models of the two-level catenary are investigated by comparing predictions of these models to those of the original two-level model. The comparison is carried out of the deflection pattern of the contact cable, of the deflection of the contact cable at the loading point, of the maximum deflection of the contact cable and of the contact force between the hangers and the contact cable.

Fig. 7 presents the deflection patterns of the contact cable as calculated by using the original model and the two simplified models. In this figure and the figures to follow, 2D, 1D and $2D_{hom}$ stand for the original two-level model, effective one-level model and homogenized two-level model. The left and right columns of figures in Fig. 7 present the patterns of the catenary with the rubber hangers and the friction hangers, respectively.

In general, Fig. 7 allows to conclude that resemblance of the three predictions is much better in the case of the friction hangers than in the case of the rubber hangers. This is because the friction hangers are much softer, which results in (i) smoother variation of the global catenary stiffness, enabling better predictions of the homogenized model and (ii) weaker coupling between the cables, enabling better predictions of the one-level model.

The effective one-level model predicts the displacement of the contact cable quite well in the vicinity of the load but fails to do so as the distance from the load grows. This failure is related to the fact that the 'far-field' pattern is governed by super-harmonics, which are much more sensitive to the structure of the catenary. The homogenized two-level model predicts the deflection pattern somewhat better than the effective one-level

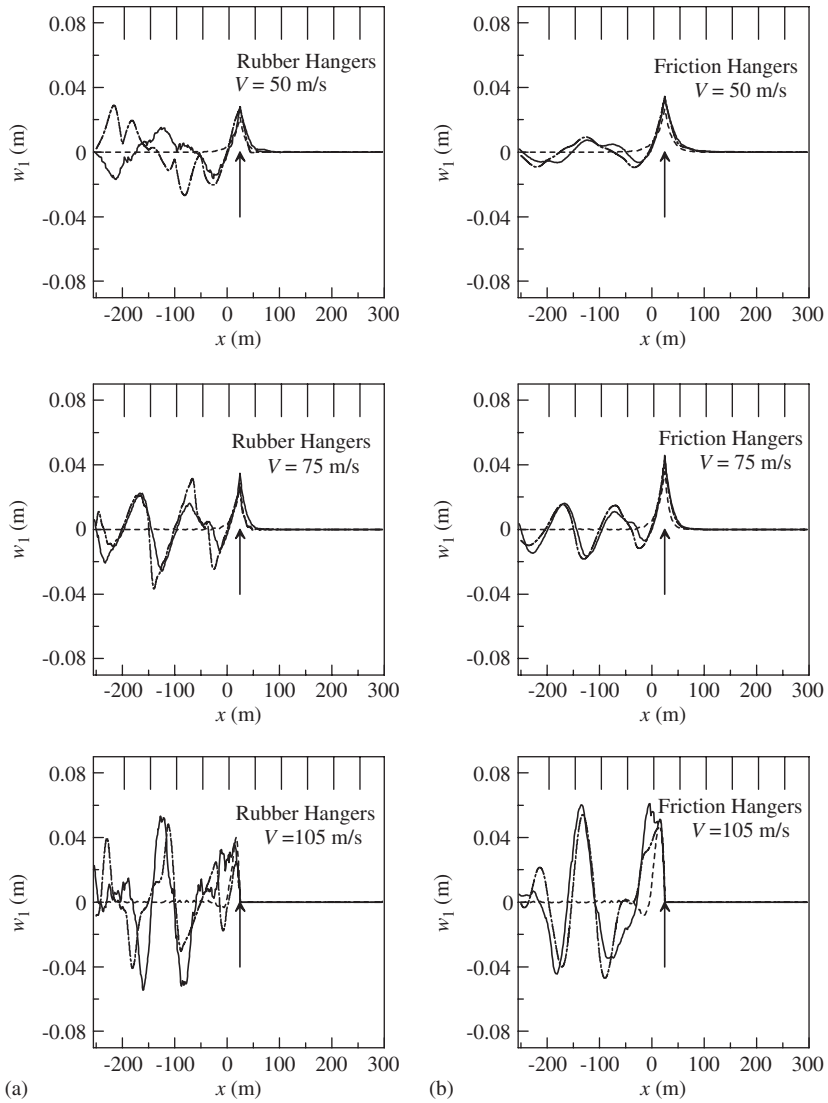

Fig. 7. Comparison of *deflection patterns* as predicted by the two-level model (2D), effective one-level model (1D) and homogenized two-level model ($2D_{hom}$). (a) Rubber hangers, (b) friction hangers. Solid line: 2D; dashed line: 1D; dashed-dotted line: $2D_{hom}$.

model. Especially good are predictions for the catenary with soft friction hangers. The stiff rubber hangers, naturally, worsen the prediction of the homogenized model.

Fig. 8 presents the displacement of the contact cable at the loading point as a function of the position of the load within the first span. This figure confirms all conclusions made on the basis of the previous figure. Additionally, one can see one more weakness of the one-level model at relatively low velocities of the load. This model cannot predict the variation of the deflection of the loading point within the span, which is especially apparent in the case of the rubber hangers (see the first two figures of the left column). The homogenized two-level model provides acceptable predictions if the load velocity is relatively low. As the velocity increases, however, it fails to predict sharp variations of the path of the loading point, which are caused by the discrete character of the hangers.

The maximum deflection of the contact cable as a function of the load velocity is presented in Fig. 9. This figure shows that the catenary with the friction hangers is much better approximated by the simplified models,

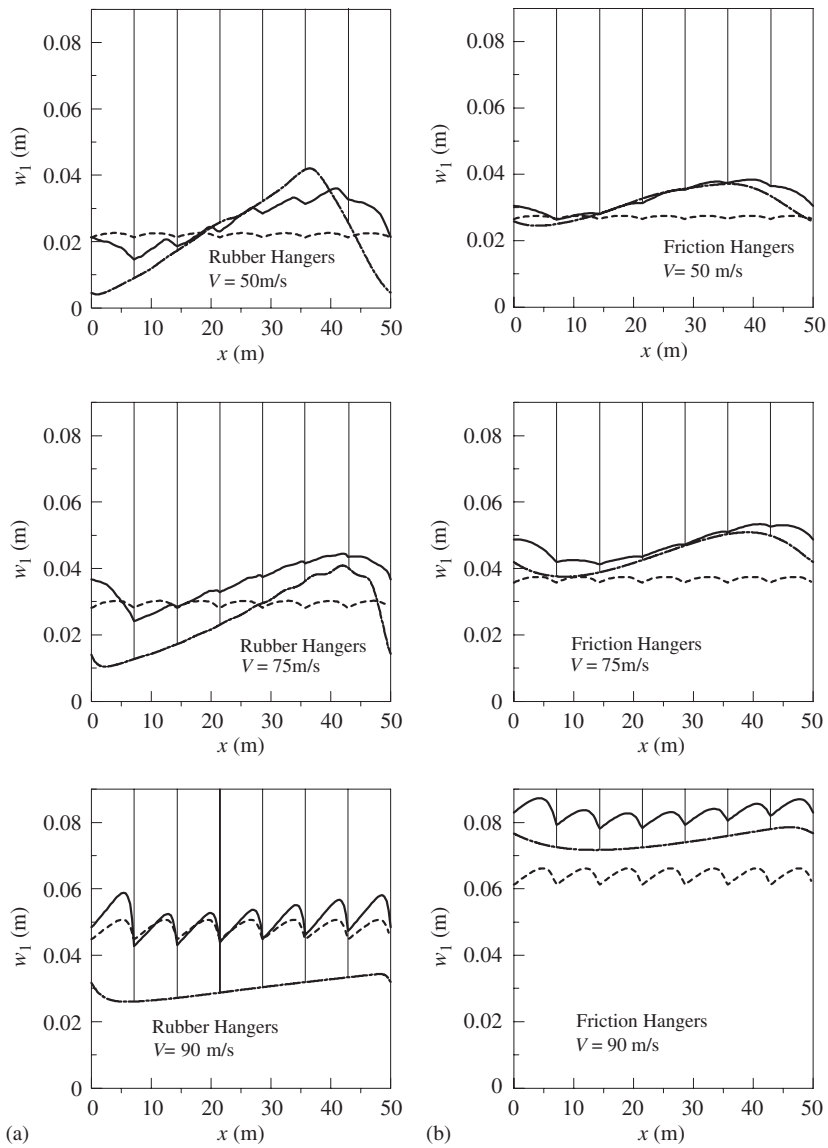

Fig. 8. Comparison of the contact cable *deflection at the loading point* as predicted by 2D, 1D, and $2D_{hom}$ models. (a) Rubber hangers, (b) friction hangers. Solid line: 2D; dashed line: 1D; dashed–dotted line: $2D_{hom}$.

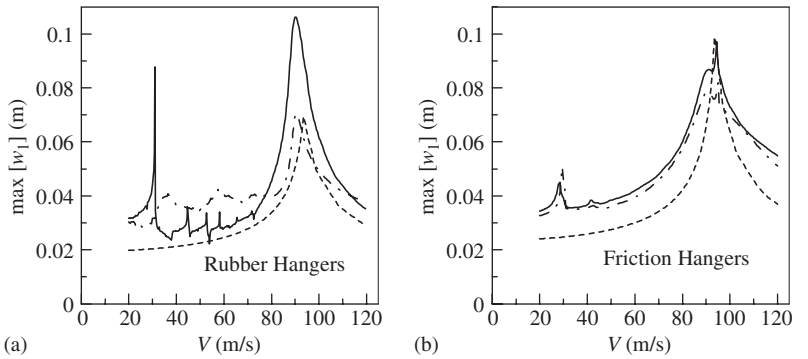

Fig. 9. Comparison of the *maximum deflection* of the contact cable as predicted by 2D, 1D, and $2D_{hom}$ models. (a) Rubber hangers, (b) friction hangers. Solid line: 2D; dashed line: 1D; dashed–dotted line: $2D_{hom}$.

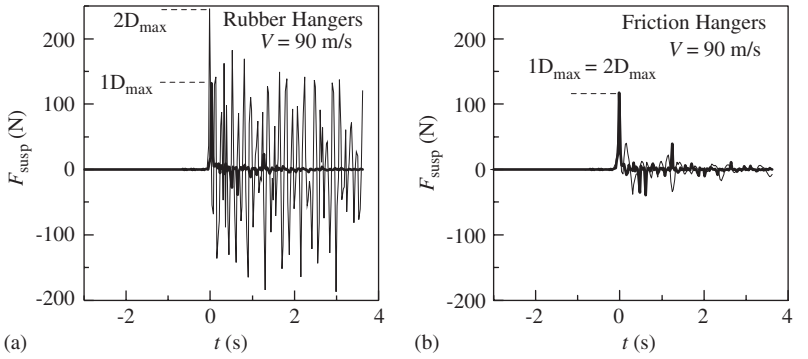

Fig. 10. Comparison of the *contact force* between the hanger at $x = 0$ and the contact cable as predicted by 2D and 1D models. (a) Rubber hangers, (b) friction hangers. Regular solid line: 2D; bold solid line: 1D.

even at the load velocities close to the critical ones. The catenary with the stiff rubber hangers, on the other hand, shows obvious deficiency of the simplified models at the critical load velocities.

The contact force between the hanger positioned at $x = 0$ and the contact cable as a function of time is shown in Fig. 10. Only the one-level model is compared to the original one, since the homogenized two-level model cannot describe this contact force. Fig. 10 shows once again that the catenary with the friction hangers can be approximated reasonably well by the simplified model. On the contrary, the one-level simplification of the catenary with the rubber hangers fails to approximate both the maximum force and the post-peak oscillations of this force.

7. Conclusions

In this paper, an analytical method has been proposed for calculating the steady-state response of a two-level catenary to a uniformly moving pantograph. This method is applicable to linear models of the catenary only, since it is based on the Fourier transformation of the problem into the frequency domain. The model, which has been considered in this paper, is composed of two strings, which are connected by lumped mass-spring-dashpot elements. These elements have been assumed to be linear elastic and to dampen proportionally to the velocity. They can be used to describe the dynamic behaviour of so-called friction damping hangers and rubber damping hangers, which are being currently tested with the aim to replace conventional suspension cables of the overhead power lines for high-speed trains.

The proposed method has been applied to study the deflection of the contact cable and the contact force between this cable and the hangers. This study has shown that the steady-state deflection pattern of the contact cable is asymmetric with respect to the loading point independently of the load velocity. The greater

this velocity, the higher is the degree of asymmetry. The shape of the cable at every time instant has a wavy character, even at the load velocities, which are considerably lower than the speed of transverse waves in the cable. At these velocities, the waves are caused solely by the periodically inhomogeneous nature of the catenary, which leads to radiation of super-harmonics, whose phase velocities are smaller than the wave speed in the cable. These relatively small phase velocities enable radiation of these harmonics by the load, whose velocity is smaller than the wave speed. The frequencies of the super-harmonics, which travel behind the load, are always lower than of those which travel in front of the load. This is a consequence of the Doppler Effect. Consequently, the latter are damped more efficiently by the viscous elements of the hangers and the displacement pattern of the contact cable looks as if the waves were radiated behind the load only.

Analysing the path of the load within a span of the catenary, it has been shown that this path is perceptibly asymmetric with respect to the middle point of this span. This asymmetry, as well as the above-described asymmetry of the deflection pattern, is a natural consequence of the wave radiation by the load. One of the important properties of the load path is that it varies sharply as the load passes a hanger. The stiffer the hanger, the sharper is this variation.

The maximum deflection of one point of the contact cable has been studied as a function of the load velocity. This maximum has been calculated over a relevant time interval, when the load is close enough to the observation point so that it causes a perceptible deflection. It has been shown that a considerable dynamic amplification of the cable response takes place if the load velocity is close to the wave speed in the cable. This is a well-known phenomenon in the dynamics of continuous and homogeneous systems subject to a moving source of excitation [14,15]. If the hangers of the catenary are stiff enough, the dynamic amplification takes place at lower velocities of the load. This effect is caused by radiation of super-harmonics and is known to arise in periodically inhomogeneous continuous systems under moving loads [4].

The contact force between a hanger and the contact cable has been analyzed, which is important for estimation of the fatigue life of the hangers. It has been shown that the higher the load speed and the stiffer the hangers, the greater is this force. The maximum of this force in time is normally reached when the load passes the hanger. After this moment, the force keeps oscillating. The amplitude and duration of these post-peak oscillations increase with the load velocity.

Two simplified models of the two-level catenary have been introduced and studied in this paper. In the first simplified model, which has been referred to as an ‘effective one-level model’, the carrying cable has been assumed infinitely stiff but effective parameters of the droppers have been introduced to account for the stiffness and damping properties of this cable. In the second model, a ‘homogenized two-level model’, the simplification has been concerned with the hangers, which have been ‘continualized’, forming a continuous and homogeneous visco-elastic connection between the two cables.

Comparing predictions of the simplified models to those of the original model, it has been shown that the one-level model is capable of a reasonable prediction of the deflection pattern in the very vicinity of the load only. At higher distances from the load, the homogenized two-level model can be used but only in the case that the hangers are not too stiff. The homogenized model cannot predict the contact force between a hanger and the contact cable. The one-level model can do so but its predictions are plausible only in the case of soft hangers.

References

[1] M. Aboshi, H. Kinoshita, Current collection characteristics and improvement methods of high-tension overhead catenary systems, *Electrical Engineering in Japan* 123 (1998) 67–76.

[2] A.V. Metrikine, S.N. Verichev, Instability of vibration of a moving oscillator on a flexibly supported Timoshenko beam, *Archive of Applied Mechanics* 71 (9) (2001) 613–624.

[3] D.J. Mead, Vibration response and wave propagation in periodic structures, *Engineering for Industry—Transactions of the American Society of Mechanical Engineers* 93 (1971) 783–792.

[4] L. Jezequel, Response of periodic systems to a moving load, *Journal of Applied Mechanics—Transactions of the American Society of Mechanical Engineers* 48 (1981) 603–618.

[5] L. Jezequel, Analysis of critical speeds of a moving load on an infinite periodically supported beam, *Journal of Sound and Vibration* 73 (1980) 606–610.

[6] C.W. Cai, Y.K. Cheung, H.C. Chan, Dynamic response of infinite continuous beams subjected to a moving force—an exact method, *Journal of Sound and Vibration* 123 (1988) 461–472.
[7] R. Bogacz, T. Krzyzinski, K. Popp, On dynamics of systems modeling continuous and periodic guideways, *Archives of Mechanics* 45 (1993) 575–593.
[8] T. Krzyzynski, The influence of viscous damping on the dynamics of periodic structures, *Zeitschrift fuer Angewandte Mathematik und Mechanik* 73 (1993) T11–T114.
[9] A.I. Vesnitskiy, A.V. Metrikine, Transition radiation in a periodically non-uniform elastic guide, *Mechanics of Solids* 28 (1993) 158–162.
[10] A.I. Vesnitskiy, A.V. Metrikine, Transition radiation in mechanics, *Physics-Uspekhi* 166 (1996) 1043–1068.
[11] P.M. Belotserkovskiy, On the oscillations of infinite periodic beams subjected to a moving concentrated force, *Journal of Sound and Vibration* 193 (1996) 705–712.
[12] L. Frýba, Vibrations of Solids and Structures Under Moving Loads, Telford, London, 1999.
[13] A.V. Metrikine, K. Popp, Vibration of a periodically supported beam on an elastic half-space, *European Journal of Mechanics A/Solids* 18 (1999) 679–701.
[14] A.V. Vostroukhov, A.V. Metrikine, Periodically supported beam on a visco-elastic layer as a model for dynamic analysis of a high-speed railway track, *International Journal of Solids and Structures* 40 (2003) 5723–5752.
[15] A.S.J. Suiker, A.V. Metrikine, R. de Borst, Dynamic behaviour of a layer of discrete particles—Part 2—response to a uniformly moving, harmonically vibrating load, *Journal of Sound and Vibration* 240 (2001) 19–39.
[16] V.L. Ginzburg, *Theoretical Physics and Astrophysics*, Pergamon Press, Oxford, 1979.